

Received November 5, 2019, accepted November 15, 2019, date of publication November 20, 2019, date of current version December 6, 2019.

Digital Object Identifier 10.1109/ACCESS.2019.2954712

# Application of Pattern Recognition to the Identification of Cross-Section Deformation Modes of Thin-Walled Structures

LEI ZHANG<sup>1</sup>, WEIDONG ZHU<sup>2</sup>, AND AIMIN JI<sup>1</sup>

<sup>1</sup>College of Mechanical and Electrical Engineering, Hohai University, Changzhou 213022, China

<sup>2</sup>Department of Mechanical Engineering, University of Maryland Baltimore County, Baltimore, MD 21250, USA

Corresponding author: Lei Zhang (leizhang@hhu.edu.cn)

This work was supported in part by the National Natural Science Foundation of China under Grant 51805144 and Grant 11772100, in part by the Natural Science Foundation of Jiangsu Province under Grant BK20170300, and in part by the Changzhou Sci&Tech Program under Grant CZ20190018.

**ABSTRACT** This paper presents a novel procedure to identify cross-section deformation modes of thin-walled structures with the application of pattern recognition. Initially, a higher order model is derived by considering an approximation of cross-section deformation by a set of basis functions, which are integrated in the governing equations and decoupled through the solution of the associated generalized eigenvalue problem. The eigenvectors obtained are deemed to inherit the attributes of structural behaviors, and thus can serve as the basis to identify deformation modes. Accordingly, these eigenvectors are further handled employing the singular value decomposition, in order to recognize the axial variation patterns of the basis functions. Next, each eigenvector is orthogonally decomposed into components corresponding to the variation patterns, with their proportional relationship, which is really pursued, being obtained and used as the weights to “assemble” basis functions to generate deformation modes. Moreover, a numbering system is proposed to hierarchically organize these deformation modes. Finally, a reduced higher order model can be obtained by updating the initial governing equations with a selective set of cross-section deformation modes. The main features lie in the capability to be numerically implemented in a simple and intuitive way and the nature to give identified deformation modes mechanical interpretation inherited from actual dynamic behaviors of thin-walled structures. The versatility of the procedure as well as the resulting beam model has been validated through both numerical examples and comparisons with other theories.

**INDEX TERMS** Thin-walled structures, cross-section deformation modes, pattern recognition, a higher order beam theory.

## I. INTRODUCTION

Thin-walled structures are widely used as structural components in various fields of engineering mainly because of their advantage of high strength to weight ratio [1], [2]. The analysis of thin-walled structures through one-dimensional models represents a simple and efficient method that has been successfully adopted. However, one-dimensional models considering the three-dimensional deformation confront some challenges in providing a rational set of deformation modes: (i) the criterion to define deformation modes should be rationalized to perform automatically but adaptable to various geometry and boundary conditions; (ii) the procedure should provide a complete set of deformation modes but with

clear structural interpretation; and (iii) the number of the deformation modes employed should be as few as possible but reproduce the structural deformation as accurately as possible. Accordingly, many attempts have been made on this subject over the years [3].

Among them, the most direct strategy is to consider the addition of deformation modes that represent specific structural behaviors. Typically, the non-uniform warping is defined by Vlasov and used to refine the displacement field of thin-walled beams [4]. From then on a number of warping functions have been proposed for different thin-walled structures [5], [6]. Besides, the demands of providing an appropriate shear distribution over the cross-section have served the study of shear correction factors, which are employed in order to enhance classic beam theories for the analysis of thin-walled structures [7]. More recently, some higher order

The associate editor coordinating the review of this manuscript and approving it for publication was Wei Wang<sup>1</sup>.

deformation modes have also been brought in to capture special boundary conditions [8]. For example, the studies of the multi-cell distortion and distortional warping due to shear-lag effects have advanced the design theory of box girders in bridge engineering [9], [10].

Another strategy is to formulate the three-dimensional model to a one-dimensional one in a mathematical way, without considering the physical interpretation. In this field, the Saint-Venant solution has been an exemplary record [11], [12]. Besides, the proper generalized decomposition method has also been used for the same reason [13]. It decomposes a three-dimensional problem as the summation of several one-dimensional functions [14]. Now it has been considered as a powerful tool to reduce the numerical complexity of thin-walled structures [15], [16]. Variational asymptotic methods represent another powerful tool, which has stepped towards the refined beam model with a transcendental accuracy [17]. Furthermore, variational asymptotic methods have been refined to carry out the variational asymptotic beam sectional analysis [18], [19], allowing deriving beam-like equations for higher order effects [20]. Meanwhile, Carrera unified formulation has been developed by considering the displacement field through Taylor or Maclaurin expansions [21], [22]. Over the past decade, it has been extended for the analysis of thin-walled structures [23], which allows to improve the accuracy on representing higher order effects for arbitrary cross-sections [24], [25].

There are also some higher order beam theories trying to provide a solution that fulfills all the objectives mentioned above. The generalized beam theory (GBT) is featured with a cross-section analysis procedure, which combines elementary deformation modes defined through kinematic concepts into GBT deformation modes [26]. The procedure is achieved by means of base changes related to the eigenvectors of the stiffness matrix. At present, GBT has been used to perform first-order [27], buckling [28], post buckling [29], vibration [30] and dynamic analyses [31] of thin-walled structures. Besides, Vieira et al. [32] have also developed a higher order theory, which initially considers the displacement field through the interpolation over the meshed cross-section [33]. Towards an efficient application, a criterion is developed to uncouple the governing equations by solving the associated polynomial eigenvalue problem [34]. The results yield several sets of non-null eigenvalues representing beam classic modes and sets of pairs and quadruplets of non-null eigenvalues corresponding to higher order modes [35].

This paper works on a procedure to identify cross-section deformation modes in a simple fashion. The derived deformation modes should be of clear hierarchy and physical interpretation. Besides, geometry and boundary conditions should be considered in the identification to truly reflect the dynamic behaviors of thin-walled structures. To this end, some special measures are taken in the procedure. Firstly, governing equations of a higher order model are derived with the displacement field approximated with basis functions, which are then decoupled by solving the associated

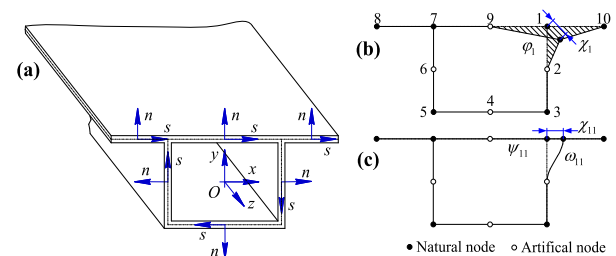
generalized eigenvalue problem. Within each eigenvector, the weights of basis functions vary along the beam axis in specific patterns. Secondly, pattern recognition is employed to handle the eigenvectors in order to recognize the variation patterns. Then these eigenvectors are decomposed into components collinear with the recognized variation patterns, with their proportional relationship being obtained and used to assemble basis functions for deformation modes. Thirdly, a numbering system is proposed to hierarchically organize the deformation modes. On this foundation, a reduced higher order model can be obtained by updating the initial governing equations with a rational set of deformation modes. In addition, the versatility of the procedure as well as the resulting beam model is validated through both numerical examples and comparisons with other theories.

## II. A HIGHER ORDER BEAM MODEL

A higher order model for thin-walled structures is presented considering the deformable cross-section. Specially, the displacement field is defined through a set of basis functions interpolated over the discretized cross-section.

### A. DISPLACEMENT FIELD

The model is supposed to be applicable to thin-walled structures with arbitrary prismatic cross-sections. For the sake of generality, a cross-section shown in Fig. 1(a) is taken as an illustrative example since it includes both open and closed profiles and possesses both symmetric and non-symmetric features. Also shown is the local reference frame  $O(s, n, z)$  adopted in each wall, with  $s$  being the coordinate along the midline,  $n$  indicating the perpendicular direction to the wall and the beam axis represented by  $z$ .



**FIGURE 1. (a) The local  $(s, n, z)$  coordinate system attached on the thin-walled structure; (b) the cross-section discretization and (c) the approximation functions adopted.**

The cross-section discretization is performed as shown in Fig. 1(b) and (c), where  $N_k = 6$  natural and  $N_a = 4$  artificial nodes are employed. Also shown is the displacement approximation along the midline, with linear Lagrange functions adopted to interpolate the axial and tangential displacement components while cubic Hermite functions are used for the normal components. Actually, the basis functions are just defined based on these shape functions to describe the variation of displacement components along  $s$ .

The displacement of an arbitrary point  $(s, z)$  on the mid-plane can be described with three components, namely

$u(s, z)$ ,  $v(s, z)$  and  $w(s, z)$  for the axial, tangential and normal components, respectively. They are approximated with a set of basis functions about  $s$ , which stem from the interpolation of nodal displacements imposed on the meshed cross-section (shown in Fig. 1). Thus,  $\mathbf{d}$ , the displacement field of the mid-plane, can be expressed as

$$\mathbf{d} = \begin{Bmatrix} u(s, z) \\ v(s, z) \\ w(s, z) \end{Bmatrix} = \begin{Bmatrix} \boldsymbol{\varphi}^T(s) \boldsymbol{\chi}(z) \\ \boldsymbol{\psi}^T(s) \boldsymbol{\chi}(z) \\ \boldsymbol{\omega}^T(s) \boldsymbol{\chi}(z) \end{Bmatrix} \quad (1)$$

where  $\boldsymbol{\varphi}$ ,  $\boldsymbol{\psi}$  and  $\boldsymbol{\omega}$  are the vectors grouping the basis functions  $\varphi(s)$ ,  $\psi(s)$  and  $\omega(s)$ , respectively;  $\boldsymbol{\chi}$  corresponds to the vector composed of their weights. Since these weights vary along  $z$ , they are also referred to as amplitude functions. The set of basis functions are written as

$$\boldsymbol{\varphi} = [\varphi_1, \varphi_2, \dots, \varphi_N]^T, \boldsymbol{\psi} = [\psi_1, \psi_2, \dots, \psi_N]^T, \\ \boldsymbol{\omega} = [\omega_1, \omega_2, \dots, \omega_N]^T \quad (2)$$

where  $\boldsymbol{\varphi}$ ,  $\boldsymbol{\psi}$  and  $\boldsymbol{\omega}$  should guarantee the continuity along  $s$ . Thus, the amplitude function vector  $\boldsymbol{\chi}$  is written as

$$\boldsymbol{\chi} = [\chi_1, \chi_2, \dots, \chi_N]^T \quad (3)$$

where  $N = 4 \times (N_k + N_a)$  since four degrees of freedom (three translations and the rotation about  $z$ ) are considered for each node.

The three-dimensional displacement field of the thin-walled structure is expressed with three components  $U(s, n, z)$ ,  $V(s, n, z)$  and  $W(s, n, z)$ . By considering the membrane and flexural behaviors of thin walls, and employing Kirchhoff's thin-plate assumption, the displacement field  $\mathbf{D}$  is obtained as

$$\mathbf{D} = \begin{Bmatrix} U(s, n, z) \\ V(s, n, z) \\ W(s, n, z) \end{Bmatrix} = \begin{Bmatrix} u(s, z) - n \frac{\partial w(s, z)}{\partial z} \\ v(s, z) - n \frac{\partial w(s, z)}{\partial s} \\ w(s, z) \end{Bmatrix} \quad (4)$$

Substitute (1) into (4); a complete kinematical description of the displacement field can be obtained as

$$\mathbf{D} = \begin{Bmatrix} \boldsymbol{\varphi}^T \boldsymbol{\chi} - n \boldsymbol{\omega}^T \boldsymbol{\chi}_{,z} \\ \boldsymbol{\psi}^T \boldsymbol{\chi} - n \boldsymbol{\omega}_{,s}^T \boldsymbol{\chi} \\ \boldsymbol{\omega}^T \boldsymbol{\chi} \end{Bmatrix} \quad (5)$$

where the subscripts  $(,s)$  and  $(,z)$  stand for the partial derivatives with respect to  $s$  and  $z$ , respectively.

The strain and stress fields are obtained under the small displacement hypothesis. In the case of small strains and by employing the Saint Venant-Kirchhoff material law, the strain field  $\boldsymbol{\varepsilon}(s, n, z) = [\varepsilon_{zz}, \varepsilon_{ss}, \gamma_{sz}]^T$  and stress field  $\boldsymbol{\sigma}(s, n, z) = [\sigma_{zz}, \sigma_{ss}, \tau_{sz}]^T$  can be expressed as

$$\boldsymbol{\varepsilon} = \mathbf{L}\mathbf{D} = \begin{Bmatrix} \boldsymbol{\varphi}^T \boldsymbol{\chi}_{,z} - n \boldsymbol{\omega}^T \boldsymbol{\chi}_{,zz} \\ \boldsymbol{\psi}_{,s}^T \boldsymbol{\chi} - n \boldsymbol{\omega}_{,ss}^T \boldsymbol{\chi} \\ \boldsymbol{\varphi}_{,s}^T \boldsymbol{\chi} + \boldsymbol{\psi}^T \boldsymbol{\chi}_{,z} - 2n \boldsymbol{\omega}_{,s}^T \boldsymbol{\chi}_{,z} \end{Bmatrix} \quad (6)$$

$$\boldsymbol{\sigma} = \mathbf{C}\boldsymbol{\varepsilon} \\ = \begin{Bmatrix} E^* (\boldsymbol{\varphi}^T \boldsymbol{\chi}_{,z} - n \boldsymbol{\omega}^T \boldsymbol{\chi}_{,zz}) + E^* \nu \left( \boldsymbol{\psi}_{,s}^T \boldsymbol{\chi} - n \boldsymbol{\omega}_{,ss}^T \boldsymbol{\chi} \right) \\ E^* \nu (\boldsymbol{\varphi}^T \boldsymbol{\chi}_{,z} - n \boldsymbol{\omega}^T \boldsymbol{\chi}_{,zz}) + E^* \left( \boldsymbol{\psi}_{,s}^T \boldsymbol{\chi} - n \boldsymbol{\omega}_{,ss}^T \boldsymbol{\chi} \right) \\ G (\boldsymbol{\varphi}_{,s}^T \boldsymbol{\chi} + \boldsymbol{\psi}^T \boldsymbol{\chi}_{,z} - 2n \boldsymbol{\omega}_{,s}^T \boldsymbol{\chi}_{,z}) \end{Bmatrix} \quad (7)$$

where  $\mathbf{L}$  and  $\mathbf{C}$  are the differential operator and the constitutive matrix, respectively;  $E^* = E/(1-\nu^2)$ ,  $G = E/(2+2\nu)$  in which  $E$  and  $\nu$  are the material elasticity modulus and Poisson coefficient, respectively.

## B. GOVERNING EQUATIONS

The thin-walled structure is supposed to be subjected to a set of distributed forces  $\mathbf{p} = [p_z, p_s, p_n]^T$ , where the elements are the force densities along  $z$ ,  $s$  and  $n$ , respectively. Thus, the structure total energy can be given as

$$\Pi = \frac{1}{2} \int_V \rho \frac{\partial \mathbf{D}^T}{\partial t} \frac{\partial \mathbf{D}}{\partial t} dV - \frac{1}{2} \int_V \boldsymbol{\varepsilon}^T \boldsymbol{\sigma} dV - \int_A \mathbf{p}^T \mathbf{d} dA \quad (8)$$

where  $V$  is the structure volume,  $\rho$  is the material density, and  $A$  is the area of the mid-plane.

The dynamic modeling of thin-walled structures involves the application of Hamilton's principle, reading (in the absence of dissipative forces)

$$\delta H = \delta \int_{t_1}^{t_2} \Pi dt = 0 \quad (9)$$

where  $H$  is the Hamiltonian, and  $t_1$  and  $t_2$  are boundary times. In the case of this paper, the principle yields the governing equations by substituting (1), (5), (6), (7) and (8) into (9) as

$$\int_0^L \mathbf{M}_1 \frac{\partial^2 \boldsymbol{\chi}}{\partial t^2} dz + \int_0^L \mathbf{M}_2 \frac{\partial^2 \boldsymbol{\chi}_{,zz}}{\partial t^2} dz \\ + \int_0^L \mathbf{K}_1 \boldsymbol{\chi} dz + \int_0^L \mathbf{K}_2 \boldsymbol{\chi}_{,z} dz \\ + \int_0^L \mathbf{K}_3 \boldsymbol{\chi}_{,zz} dz + \int_0^L \mathbf{K}_4 \boldsymbol{\chi}_{,zzzz} dz = \int_0^L \mathbf{P} dz \quad (10)$$

where related terms are given by

$$\mathbf{M}_1 = \int_{\Omega} \rho (\boldsymbol{\varphi} \boldsymbol{\varphi}^T + \boldsymbol{\psi} \boldsymbol{\psi}^T + \boldsymbol{\omega} \boldsymbol{\omega}^T + n^2 \boldsymbol{\omega}_{,s} \boldsymbol{\omega}_{,s}^T) d\Omega \\ \mathbf{M}_2 = \int_{\Omega} \rho n^2 \boldsymbol{\omega} \boldsymbol{\omega}^T d\Omega \quad (11)$$

$$\mathbf{K}_1 = \int_{\Omega} [E^* (\boldsymbol{\psi}_{,s} \boldsymbol{\psi}_{,s}^T + n^2 \boldsymbol{\omega}_{,ss} \boldsymbol{\omega}_{,ss}^T) + G \boldsymbol{\varphi}_{,s} \boldsymbol{\varphi}_{,s}^T] d\Omega \quad (12)$$

$$\mathbf{K}_2 = \int_{\Omega} [E^* \nu (\boldsymbol{\varphi} \boldsymbol{\psi}_{,s}^T + \boldsymbol{\psi}_{,s} \boldsymbol{\varphi}^T) + G (\boldsymbol{\psi} \boldsymbol{\varphi}_{,s}^T + \boldsymbol{\varphi}_{,s} \boldsymbol{\psi}^T)] d\Omega \quad (13)$$

$$\mathbf{K}_3 = \int_{\Omega} [E^* (\boldsymbol{\varphi} \boldsymbol{\varphi}^T + \nu n^2 \boldsymbol{\omega} \boldsymbol{\omega}_{,ss}^T + \nu n^2 \boldsymbol{\omega}_{,ss} \boldsymbol{\omega}^T) + G (4n^2 \boldsymbol{\omega}_{,s} \boldsymbol{\omega}_{,s}^T + \boldsymbol{\psi} \boldsymbol{\psi}^T)] d\Omega \quad (14)$$

$$\mathbf{K}_4 = \int_{\Omega} E^* n^2 \boldsymbol{\omega} \boldsymbol{\omega}^T d\Omega \quad (15)$$

$$\mathbf{P} = \int_{\Gamma} (p_z \boldsymbol{\varphi}^T + p_s \boldsymbol{\psi}^T + p_n \boldsymbol{\omega}^T) ds \quad (16)$$

with parameters  $L$  and  $\Omega$  indicating the beam length and the cross-section midline, respectively.

Theoretically, the governing equations (10) can serve well for dynamic modeling of thin-walled structures. However, the displacement field is purely based on kinematic concepts, and the large number of basis functions adopted hinders efficient computation. Accordingly, further improvements should be made to refine the model by providing a rational set of cross-section deformation modes.

### III. IDENTIFICATION OF DEFORMATION MODES

The identification of cross-section deformation modes is based on the handling of generalized eigenvectors related to the dynamic governing equations, thus being deemed to inherit mechanical characteristics of thin-walled structures.

#### A. EIGENVECTORS

The generalized eigenvalue problem related to the dynamic governing equations (10) is solved to obtain the eigenvectors using the finite element method. As a result, the eigenvectors are derived and grouped in a matrix  $\Phi$  as

$$\Phi = [\boldsymbol{\chi}^{(1)}, \boldsymbol{\chi}^{(2)}, \dots, \boldsymbol{\chi}^{(k)}, \dots, \boldsymbol{\chi}^{(N)}] \quad (17)$$

where the superscript  $(k)$  is the order of an eigenvector. Notice that an eigenvector  $\boldsymbol{\chi}^{(k)}$  has been grouped with  $N$  amplitude functions as  $\boldsymbol{\chi}^{(k)} = [\boldsymbol{\chi}_1(z), \boldsymbol{\chi}_2(z), \dots, \boldsymbol{\chi}_N(z)]^T$  in advance. Since each amplitude function has been discretized into  $N_e$  node values along  $z$ , the amplitude function  $\boldsymbol{\chi}_i(z)$  can be expressed in a discretization form as

$$\boldsymbol{\chi}_i = [\chi_i(1), \chi_i(2), \dots, \chi_i(N_e)]^T. \quad (18)$$

In other words, an eigenvector  $\boldsymbol{\chi}^{(k)}$  is actually spanned with  $N$  amplitude function vectors  $\boldsymbol{\chi}_i(k)$  that further contain  $N_e$  node values. Thus, it can be rewritten in a matrix form as

$$\boldsymbol{\chi}^{(k)} = [\boldsymbol{\chi}_1^{(k)}, \boldsymbol{\chi}_2^{(k)}, \dots, \boldsymbol{\chi}_N^{(k)}] \in \mathbb{R}^{N_e \times N} \quad (19)$$

where each column represents the axial variation of an amplitude function. More precisely, the eigenvector  $\boldsymbol{\chi}^{(k)}$  is newly reformed as an “eigen matrix”.

In fact, the eigen matrix (19) has uncoupled the kinematic variables in (10), and provides an access to have an insight of the relations among basis functions: they are deemed to possess the information to conduct the assemblage of basis functions. Within each eigenvector, axial variation patterns of amplitude functions correspond to structural behaviors. The procedure comes into the clustering and classification, which is the strong suit of pattern recognition.

#### B. PATTERN RECOGNITION

The pattern recognition aiming at the clustering of variation patterns involves the singular value decomposition of the eigen matrix. By means of the principal pattern analysis,

the variation patterns can be derived in the form of basis vectors. The identification of deformation modes is then sorted out by decomposing the amplitude functions into components collinear with the basis vectors and by assembling basis functions employing the same set of weights derived from the decomposing procedure.

For a better presentation, the procedure above is carried out on the thin-walled structure shown in Fig. 1. Without special consideration, the cross-section is set to have a height of  $h = 0.6$  m, a bottom width of  $b = 0.8$  m, a flange width of  $c = 0.3$  m and a wall thickness of  $e = 0.03$  m. The structure is cantilevered, with an axial length of  $L = 6.4$  m. Material parameters are  $E = 200$  GPa,  $\nu = 0.3$  and  $\rho = 7830$  kg/m<sup>3</sup>. The generalized eigenvalue problem associated with the homogenous form of (10) has been solved in advance by discretizing the beam into 40 quadratic finite elements. The derived eigenvectors have also been rewritten in the form of the eigen matrix (19).

Pattern recognition of the amplitude functions actually comes to the low-rank approximation of the eigen matrix. Here  $\boldsymbol{\chi}^{(k)}$  is generally not a square matrix. However, the theorem of Autonee-Eckart-Young is applicable to an arbitrary complex rectangular matrix. As a result,  $\boldsymbol{\chi}^{(k)}$  is decomposed as

$$\boldsymbol{\chi}^{(k)} = \mathbf{U}^{(k)} \boldsymbol{\Sigma}^{(k)} \mathbf{V}^{(k)} \in \mathbb{R}^{N_d \times N}, \mathbf{U}^{(k)} \in \mathbb{R}^{N_d \times N_d} \quad (20)$$

where related matrices are given by

$$\mathbf{U}^{(k)} = [\mathbf{u}_1^{(k)}, \mathbf{u}_2^{(k)}, \dots, \mathbf{u}_N^{(k)}], \boldsymbol{\Sigma}^{(k)} = \begin{bmatrix} \boldsymbol{\Sigma}_1 & \mathbf{0} \\ \mathbf{0} & \mathbf{0} \end{bmatrix}, \quad \boldsymbol{\Sigma}_1^{(k)} = \text{diag}(\sigma_1^{(k)}, \sigma_2^{(k)}, \dots, \sigma_r^{(k)}) \quad (21)$$

with the following relations adopted

$$\sigma_1^{(k)} \geq \sigma_2^{(k)} \geq \dots \geq \sigma_r^{(k)}, r = \text{rank}[\boldsymbol{\chi}^{(k)}]. \quad (22)$$

The first  $r$  columns  $\mathbf{u}_i^{(k)}$  of  $\mathbf{U}^{(k)}$  are orthogonal basis vectors of the column space of  $\boldsymbol{\chi}^{(k)}$ . All of them can be used to cluster the variation pattern of amplitude functions, but only the “effective” ones are meaningful for the identification of deformation modes. It depends on the effective rank  $p$ , the maximum integer that satisfies the following relation

$$\mu_p^{(k)} = [\sigma_p^{(k)}]^2 / \sum_{j=1}^r [\sigma_j^{(k)}]^2 \geq \mu_0 \quad (23)$$

where  $\mu$  is the contribution value of a basis vector. The threshold  $\mu_0$  can be determined as 0.001 for most cases.

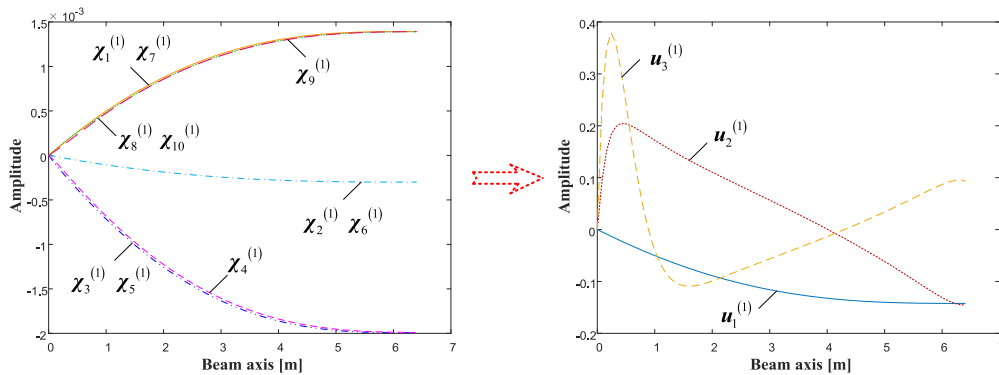
In practice, each eigen matrix is divided into two submatrices to process out-of-plane and in-plane deformation modes separately. The step can be expressed as

$$\boldsymbol{\chi}^{(k)} = \begin{bmatrix} \boldsymbol{\chi}_{\text{out}}^{(k)} \\ \boldsymbol{\chi}_{\text{in}}^{(k)} \end{bmatrix} \in \mathbb{R}^{N_e \times N}, \boldsymbol{\chi}_{\text{out}}^{(k)} \in \mathbb{R}^{N_e \times N_{\text{out}}}, \boldsymbol{\chi}_{\text{in}}^{(k)} \in \mathbb{R}^{N_e \times N_{\text{in}}} \quad (24)$$

where  $N_{\text{out}} = N/4$  and  $N_{\text{in}} = 3 \times N/4$  are the numbers of out-of-plane and in-plane amplitude functions, respectively.

**TABLE 1.** Contribution values of principal variation patterns for the first-order eigenvector of the illustrative thin-walled structure.

Pattern number	1	2	3	4	5	6	7	8	9	10
Singular value	0.032775	0.000152	0.000055	→0	→0	→0	→0	→0	→0	→0
Contribution value	0.999976	0.000021	0.000003	→0	→0	→0	→0	→0	→0	→0

**FIGURE 2.** The three variation patterns obtained from the pattern recognition of the first-order eigenvector of the illustrative thin-walled structure.

Take the pattern recognition of out-of-plane amplitude functions as an example to illustrate the procedure. With the singular value decomposition of  $\chi_{out}^{(1)}$ , all of its ten singular values are obtained and exhibited in Table 1. The effective rank is determined as  $p = 3$  through the analysis of contribution values (here the threshold is determined as 0.000001) employing (23). Thus, the first three columns of  $\mathbf{U}^{(1)}$ , i.e.  $\mathbf{u}_i^{(1)}$  ( $i = 1, 2, 3$ ), are selected as the principal variation patterns.

Fig. 2 shows the three principal patterns obtained from the pattern recognition of the ten out-of-plane amplitude function vectors. Not surprisingly, three orthogonal waves are presented in Fig. 2(b). The result supports that three principal variation patterns play dominant roles in performing the structural behaviors. Actually, each of them represents a cross-section deformation mode. The next step is to decompose all the amplitude functions and classify the resulting components into the three recognized variation patterns.

### C. ASSEMBLAGE OF BASIS FUNCTIONS

With principal variation patterns recognized, it is workable to decompose any amplitude function into components collinear with basis vectors. To ensure the orthogonality, an amplitude function component  $[\chi_i^{(k)}]_j$  corresponding to the principal component  $\mathbf{u}_j^{(k)}$  is decomposed from  $\chi_i^{(k)}$ , reading

$$[\chi_i^{(k)}]_j = \lambda_{i,j}^{(k)} \mathbf{u}_j^{(k)}, \lambda_{i,j}^{(k)} = \frac{\text{dot}(\chi_i^{(k)}, \mathbf{u}_j^{(k)})}{\text{dot}(\mathbf{u}_j^{(k)}, \mathbf{u}_j^{(k)})} \quad (25)$$

where  $\text{dot}()$  is the inner product of the two vectors, and  $\lambda_{i,j}$  is the weight of  $[\chi_i^{(k)}]_j$  when  $\mathbf{u}_j^{(k)}$  acts as the basis vector.

In general, a set of  $N \times p$  component weights  $\lambda_{i,j}$  ( $i = 1, 2, \dots, N, j = 1, 2, \dots, p$ ) can be determined for each eigen

matrix  $\chi^{(k)}$  through the decomposition procedure. They are organized into a matrix  $\lambda^{(k)}$  as

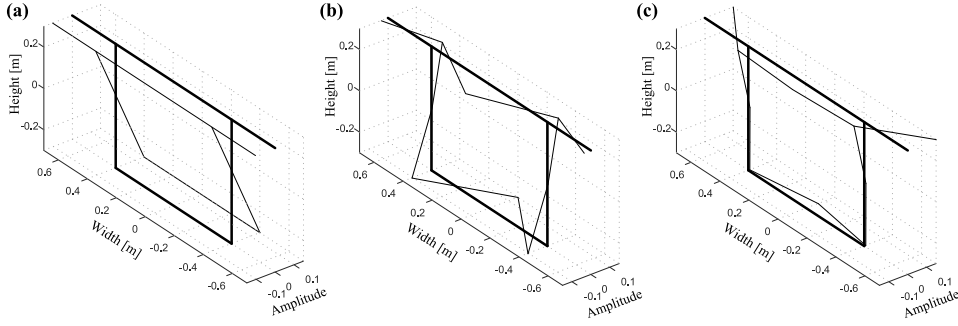
$$\lambda^{(k)} = \begin{bmatrix} \lambda_{1,1}^{(k)} & \lambda_{1,2}^{(k)} & \cdots & \lambda_{1,p}^{(k)} \\ \lambda_{2,1}^{(k)} & \lambda_{2,2}^{(k)} & \cdots & \lambda_{2,p}^{(k)} \\ \vdots & \vdots & \ddots & \vdots \\ \lambda_{N,1}^{(k)} & \lambda_{N,2}^{(k)} & \cdots & \lambda_{N,p}^{(k)} \end{bmatrix} = [\lambda_1^{(k)}, \lambda_2^{(k)}, \dots, \lambda_p^{(k)}] \quad (26)$$

where  $\lambda_j^{(k)}$  is the weight vector corresponding to a principal variation pattern  $j$  ( $j = 1, 2, \dots, p$ ) derived from the eigen matrix  $k$ . Actually, they are also the weights of the set of basis functions that can be assembled for a cross-section deformation mode, since the amplitude function itself is the weight of a basis function. However, it should be noticed that not all the weight vectors are effective, since some deformation modes may be recurrent in different patterns. To ensure the independency, a newly identified weight vector  $\lambda_j^{(k)}$  should retain the full column rank of  $\lambda^{(k)}$ , reading

$$\begin{aligned} \text{rank}[\lambda^{(k)}] &= \text{rank}[\lambda_1^{(k)}, \lambda_2^{(k)}, \dots, \lambda_i^{(k)}, \lambda_j^{(k)}] \\ &= \text{rank}[\lambda_1^{(k)}, \lambda_2^{(k)}, \dots, \lambda_i^{(k)}] + 1 = r^{(k)} \end{aligned} \quad (27)$$

where  $r^{(k)}$  is the column rank of the weight matrix  $\lambda^{(k)}$ , with  $r^{(k)} \leq p$ . If not, the new weight vector should be deleted from the final weight matrix.

With the application of the decomposition procedure to a certain amount of eigen matrices  $\chi^{(k)}$ , a set of  $\lambda^{(k)}$  can be derived to determine a set of cross-section deformation modes. They are further organized into a



**FIGURE 3.** The three out-of-plane deformation modes identified from the first-order eigenvector of the illustrative thin-walled structure.

matrix  $\Lambda$  as

$$\Lambda = [\lambda^{(1)}, \lambda^{(2)}, \dots, \lambda^{(N_s)}] \quad (28)$$

where  $N_s$  is the number of eigen matrices being processed. Its value depends on the required accuracy of the higher order model. In a special case where a complete set of cross-section deformation modes are needed,  $N_s$  is determined by

$$N_s = \min \left\{ N_s \mid \sum_{k=1}^{k=N_s} r^{(k)} = N \right\} \quad (29)$$

which also indicates that the number of identified cross-section deformation modes will not exceed the number of basis functions. However, it is also possible that some cross-section deformation modes may be recurrent in different eigenvectors. Therefore, one should ensure the orthogonality within the columns of the final weight matrix  $\Lambda$ . This means  $\Lambda$  should be of full column rank by deleting the columns collinear with existing ones.

The final weight matrix  $\Lambda$  demonstrates the compositions of cross-section deformation modes. Or rather, it provides the sets of weights to assemble basis functions for the cross-section deformation modes, with

$$\begin{aligned} \Phi_i(s) &= \sum_{j=1}^{N_{out}} [\lambda_{i,j} \varphi_j(s)], \quad \Psi_i(s) = \sum_{j=N_{out}+1}^N [\lambda_{i,j} \psi_j(s)], \\ \Upsilon_i(s) &= \sum_{j=N_{out}+1}^N [\lambda_{i,j}^{(k)} \omega_j(s)] \end{aligned} \quad (30)$$

where  $\lambda_{i,j}$  is the element of the weight matrix  $\Lambda$ , with  $\lambda_{i,j} = \Lambda(i, j)$ ;  $\Phi_i(s)$ ,  $\Psi_i(s)$  and  $\Upsilon_i(s)$  are the axial, tangential and normal components of the shape function of deformation mode  $i$ , respectively.

In practice, out-of-plane and in-plane amplitude function vectors are separately decomposed, which results in the

identification of at most  $N_{out}$  out-of-plane and  $N_{in}$  in-plane deformation modes. Here take the decomposition of out-of-plane amplitude functions of the first-order eigenvector as an example to illustrate the procedure. By employing the decomposition procedure shown in (25), the weigh matrix for the out-of-plane amplitude functions is obtained as (31).

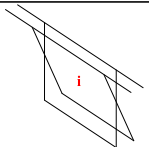
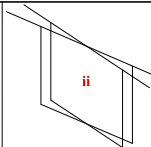
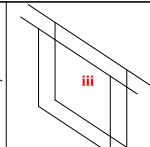
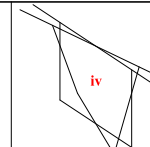
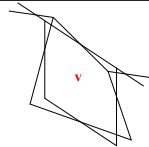

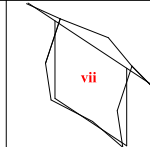
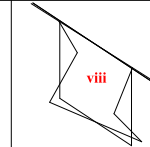
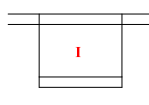
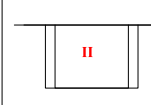
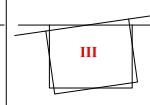
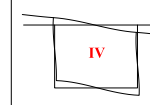
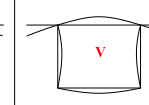
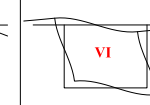
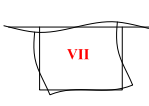
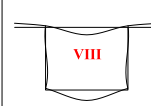
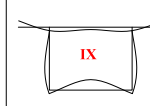
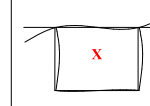
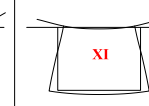
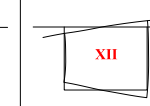
The result in (31), as shown at the bottom of this page, provides three sets of weights for the assemblage of three cross-section deformation modes. By employing the assemblage procedure shown in (30), three identified out-of-plane deformation modes are obtained and shown in Fig. 3. The results make it clear that the first principal variation pattern corresponds to classic bending about the minor axis, and the other two represent warping modes concomitant with the classic bending but with relatively smaller contribution values. In this sense, the identified cross-section deformation modes naturally possess structural interpretation. Besides, the hierarchy is also embodied through their contribution values.

The procedure above is carried out on the first  $N_s$  eigenvectors one by one, until the number of identified cross-section deformation modes satisfies the requirements. It should be pointed out that the procedure can be carried out automatically with the help of a computer in a more efficient way. Finally, because the deformation modes are assembled by handling eigenvectors, their amplitudes of shape functions should be normalized after the identification. The normalized criteria are simply expressed as rendering the maximum value of each deformation mode shape function to be 1.

#### D. NUMBERING OF DEFORMATION MODES

In the above section, basis functions are assembled to generate a set of cross-section deformation modes that are of physical interpretation since they stem from the eigenvectors of the governing equations. Moreover, the sequence of

$$\lambda_{out}^{(1)} = \begin{bmatrix} -0.6987 & 0.1506 & 1.000 & 1.000 & 1.000 & 0.1506 & -0.6987 & -0.6987 & -0.6987 & -0.6987 \\ 0.3765 & 0.0112 & -0.6957 & 1.000 & -0.6957 & 0.0112 & 0.3765 & -0.2448 & -0.8508 & -0.2448 \\ -0.3691 & 0.0555 & 0.0494 & 0.4200 & 0.0494 & 0.0555 & -0.3691 & 1.000 & -0.4879 & 1.000 \end{bmatrix}^T \quad (31)$$

Out-of-plane modes						
						
In-plane modes						
						

**FIGURE 4.** The numbering of cross-section deformation modes identified for the illustrative thin-walled structure by employing the proposed procedure.

eigenvectors and the contribution values of principal components reflect the priority of identified deformation modes. Thus, the proposed procedure is expected to organize the deformation modes hierarchically, thereby being conducive to develop reduced higher order models.

To this end, it is essential to propose a numbering system that orders the identified deformation modes considering their priority. Generally, the numbering system divides the cross-section deformation modes into two families for both out-of-plane and in-plane modes: the ones with contribution values bigger than 0.5 are classified into Dominant family, and the ones with smaller contribution values belong to Secondary family. The members of Dominant family occupy the first row according to the sequence they are identified, while the members of Secondary family are arranged in the subsequent rows in a descending order of their contribution values. The numbering is carried out row by row, reflecting the hierarchy of cross-section deformation modes. Fig. 4 shows the numbering of the identified deformation modes for the illustrative thin-walled structure, where eight out-of-plane modes (modes i to viii) and twelve in-plane modes (mode I to XII) are identified and ordered. Among them, modes i to iv and I to VI are Dominant family members, while modes v to viii and VII to XII belong to Secondary family.

#### IV. ILLUSTRATIVE EXAMPLES AND DISCUSSION

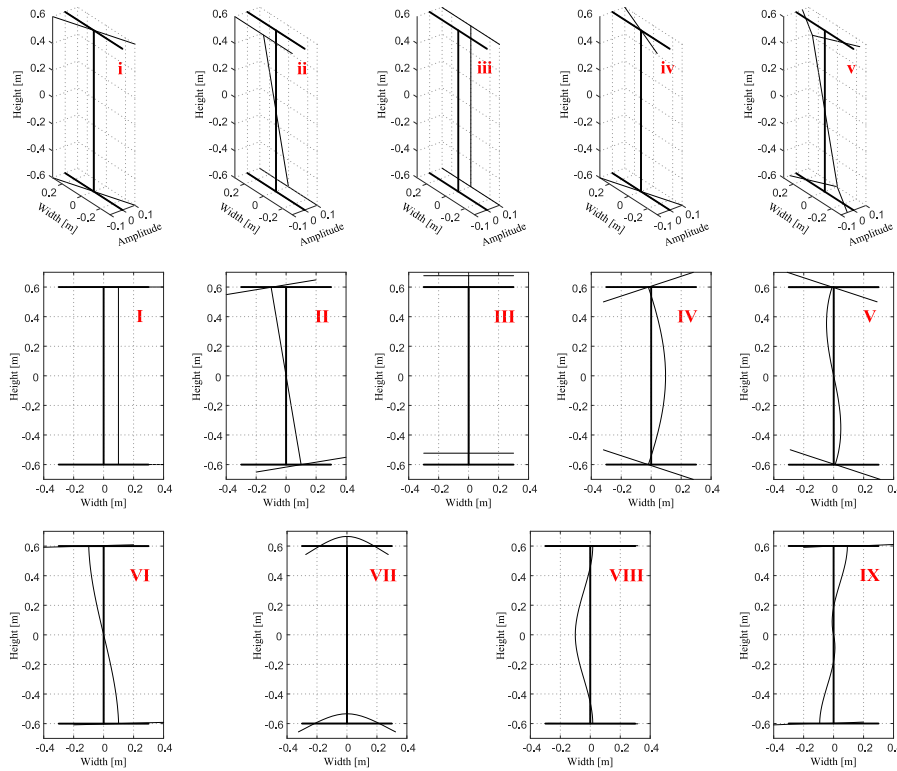
In order to illustrate the versatility of the proposed procedure, numerical examples are carried out on a typical I-shaped cross-section. Moreover, free vibration analysis of the thin-walled structures is implemented to test the accuracy and efficiency of the resulting higher order beam models.

##### A. BEAM CROSS-SECTION ANALYSIS

In this part the proposed procedure is verified concerning the capability to provide a rational set of cross-section deformation modes. Its performance is to be evaluated through the comparison with other theories. Here a steel beam with an I-shaped cross-section is considered. The cross-section has a web with dimensions  $1.2 \text{ m} \times 0.02 \text{ m}$  and two flanges with dimensions  $0.6 \text{ m} \times 0.05 \text{ m}$ . The material parameters are  $E = 210 \text{ GPa}$ ,  $\nu = 0.3$  and  $\rho = 7850 \text{ kg/m}^3$ , and the structure is cantilevered with a beam length of  $L = 8 \text{ m}$ .

The discretization of the cross-section midline with six natural nodes and one artificial node on the web results in the identification of a set of deformation modes by handling the first ten eigenvectors with the proposed procedure. They are displayed in Fig. 5, including five out-of-plane and nine in-plane deformation modes. Obviously, all the six classic modes have been captured. These deformation modes can be further classified into two families according to their participation: Dominant family including modes i, ii, iii, iv, I, II, III, IV and V, and Secondary family including modes v, VI, VII, VIII and IX. Generally, these deformation modes are adequate to form a higher order model being accurate enough for most cases in engineering. If more deformation modes with lower priority are needed in special cases, one can just handle more eigenvectors using the proposed procedure. This advantage is the conduciveness to obtain a selective number of cross-section deformation modes according to the actual needs, instead of calculating all of them from the beginning in any case. In this respect, the proposed procedure is more efficient in adapting different demands.

For comparison, the cross-section being discretized with the same seven nodes is studied using the GBT cross-section analysis [36], with the first thirteen deformation modes



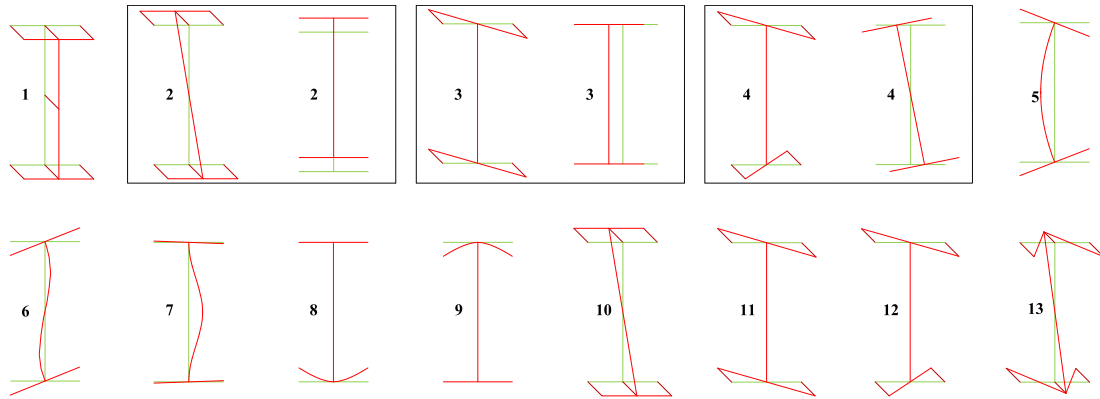
**FIGURE 5.** The cross-section deformation modes of the I-shaped cross-section beam identified with the proposed procedure.

derived and exhibited in Fig. 6. The results support that the proposed procedure agrees well with GBT, particularly concerning the out-of-plane modes. The only difference between the two sets of out-of-plane modes is the priority assignment of the classic modes, which can be attributed to the evaluation mechanism. In fact, the priority assignment of the proposed procedure may be more reasonably confined to the boundary condition of the illustrative example. However, it will not affect the accuracy or efficiency of the beam model since any classic mode is essential for a higher order model. On the other hand, some in-plane and out-of-plane modes are tied together to describe structural behaviors related to classic flexure and rotation in GBT, while they are identified separately in the proposed approach. The difference in format is irrelevant to the model accuracy, since modes 2, 3, 4, 10, 11 and 12 tied together in GBT are just equal to the linear combination of the identified modes i, ii, iv, I, II and III. Of course, GBT modes may have the advantage of employing fewer deformation modes in some cases. What actually matters is the difference between the two sets of in-plane deformation modes. For example, modes VI and VII are not optional among the first thirteen GBT deformation modes. Though the combination of modes 8 and 9 can replace mode VII, it risks the lack of a clear mechanical interpretation, while mode VII represents a structural behavior that can be directly observed in the vibration modes of the thin-walled structure. The absence of mode VI may reveal the diversity in

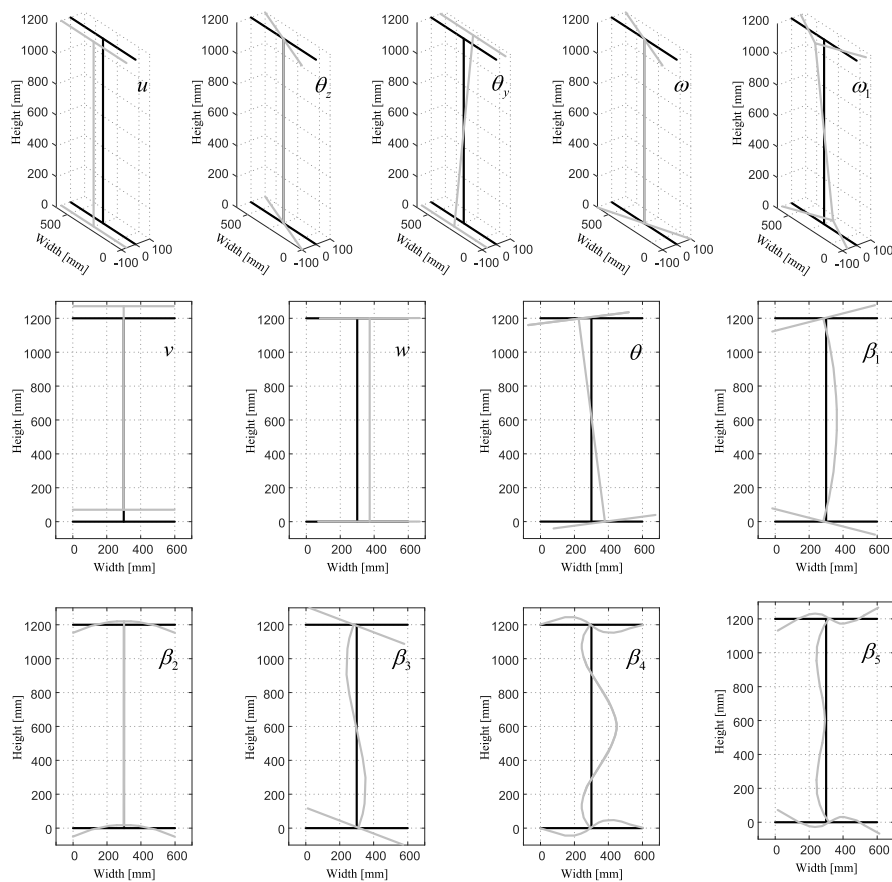
determining deformation modes for different beam theories to describe the structural deformation related to beam torsion.

For further comparison, the first 5 out-of-plane and 8 in-plane deformation modes of the same I-shaped cross-section are also obtained employing another higher order theory [35]. Here the same cross-section discretization is employed, and the identification of out-of-plane and in-plane deformation modes is separately implemented, being similar to the proposed procedure. Regarding the final results presented in Fig. 7, there are more similarities between the two theories. For example, the priority assignment of the deformation modes related to  $v$  and  $w$  in Fig. 7 are the same as that in Fig. 5. And mode VII can serve as an alternative to mode  $\beta_2$  in Fig. 7. Besides, the phenomenon that twelve of all the fourteen identified deformation modes in Fig. 5 can be found in Fig. 11 also supports that the two theories agree well with each other, although the priority assignments of two systems are not fully consistent.

Generally, the results confirm that the proposed procedure can capture the cross-section deformation modes of an I-shaped cross-section in a simple and general fashion. The derived deformation modes are roughly consistent with both GBT and another higher order theory though there are some differences. Moreover, the proposed procedure may have an advantage in providing deformation modes with physical interpretation since they stem from actual vibration modes of thin-walled structures. The results suggest that the



**FIGURE 6.** The first thirteen GBT deformation modes of the I-shaped cross-section identified with GBTUL 2.0 [36].



**FIGURE 7.** The first five out-of-plane and eight in-plane deformation modes of the I-shaped cross-section identified with another higher order theory [35].

proposed procedure is capable of considering the structural geometry, material parameters and boundary conditions in determining deformation modes. The differences among the three theories also reveal the particularity of the cross-section deformation modes that stem from the structural dynamic behaviors. Further studies may be needed to assess the effects in influencing the dynamic modeling of thin-walled structures.

## B. BEAM LONGITUDINAL ANALYSIS

In this part the same thin-walled structure is modeled for free vibration analysis, in order to verify the performance of the identified cross-section deformation modes in reproducing the structural behaviors. The beam is discretized into 40 proposed quadratic finite elements equally distributed along the axis. Meanwhile, its three-dimensional shell model is also built in the commercial software ANSYS 17.0 considering a

TABLE 2. Comparison between the proposed theory and ANSYS shell 181 concerning the first 10 natural frequencies of the I-shaped beam.

Mode number	Anslys shell	Initial beam (28 modes)		Classic beam (6 modes)		Proposed beam 1 (9 modes)		Proposed beam 2 (13 modes)	
	Frequency [Hz]	Frequency [Hz]	Relative error [%]	Frequency [Hz]	Relative error [%]	Frequency [Hz]	Relative error [%]	Frequency [Hz]	Relative error [%]
1	6.491	6.658	2.57	6.814	4.98	6.690	3.07	6.687	3.02
2	8.637	8.796	1.84	/	/	9.006	4.27	8.807	1.97
3	22.15	22.19	0.18	23.06	4.11	23.06	4.11	22.31	0.72
4	27.83	26.93	-3.23	/	/	27.69	-0.50	26.95	-3.16
5	36.31	36.51	0.55	/	/	38.48	5.98	37.13	2.26
6	44.54	45.57	2.31	42.36	-4.89	47.03	5.59	45.65	2.49
7	49.76	48.89	-1.75	/	/	50.89	2.27	49.49	-0.54
8	53.17	52.24	-1.75	/	/	53.09	-0.15	52.97	-0.38
9	60.83	59.46	-2.25	/	/	64.22	5.57	59.74	-1.79
10	69.72	68.01	-2.45	/	/	69.36	-0.52	68.10	-2.32

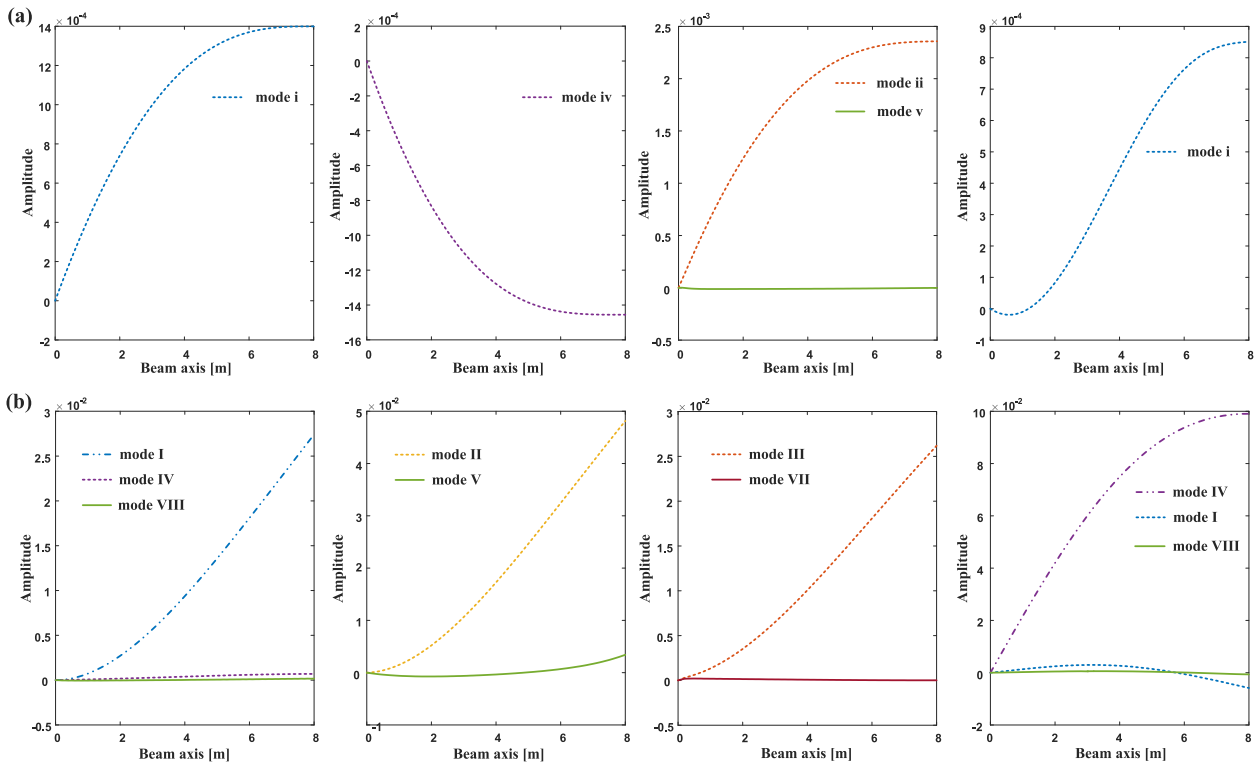


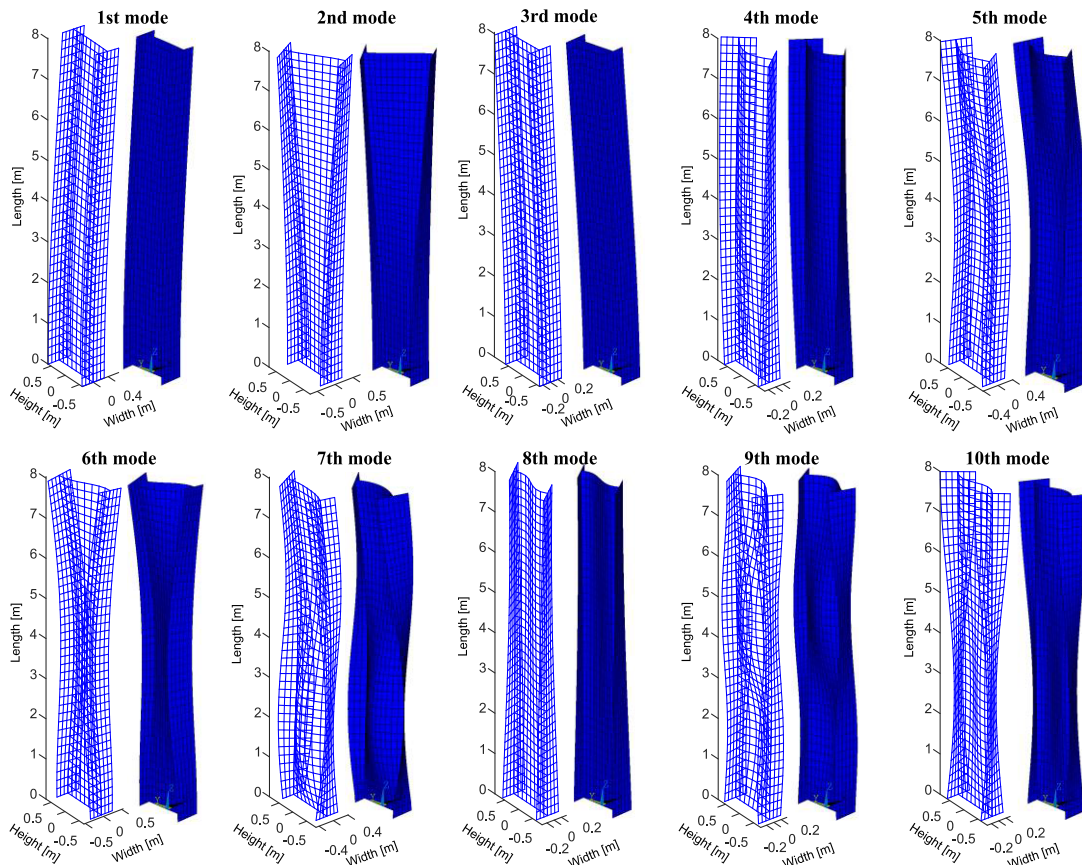
FIGURE 8. The amplitude functions of the identified cross-section deformation modes varying along the beam axis concerning the first four eigenvectors: (a) the out-of-plane modes, and (b) the in-plane modes.

mesh of 24 and 40 Shell 181 elements over the cross-section and along the beam axis, respectively.

Comparisons regarding the natural frequencies are carried out first to verify the accuracy and efficiency of the proposed model. Here several sets of deformation modes are selected from the first thirteen ones illustrated in Fig. 5 by considering the hierarchy, and then used to formulate the corresponding higher order beam models, respectively. The first set contains only six classic modes and yields the classic beam model. The second set consists of all the nine Dominant modes and forms the proposed beam model 1. The third set includes all the thirteen deformation modes and yields the proposed beam model 2. And as a reference, all the twenty-eight basis

functions are used to form the initial beam model, which represents the upper limit of accuracy of the proposed models.

Table 2 shows the results, where the relative errors are calculated based on the assumption that the values derived through ANSYS shell model are exact enough. There is a clear trend of gradual improvement of the model accuracy concerning the natural frequencies when the number of deformation modes employed increases. It is also noticeable that the proposed beam model 1 has a good agreement with the numerical results obtained from the ANSYS shell model, while the classic beam model is not competent to capture the structural behaviors even for the first two natural frequencies. Meanwhile, the results support the point that it is essential to



**FIGURE 9.** Comparison between the proposed model and the ANSYS shell model concerning the first ten vibration modes of the thin-walled beam with an I-shaped cross-section.

consider cross-section deformation modes in the modeling of thin-walled structures. One should have also noticed that the set of Dominant modes have been able to formulate a higher order model to catch all the first ten natural frequencies of a thin-walled structure. The relative errors can be further reduced to less than 3.2% when the other four Secondary modes are added into the model. The results confirm the accuracy of the proposed model as well as the hierarchy of the deformation modes. Besides, one should bear in mind that the results obtained with a mesh of 40 proposed beam elements are compared with those derived with 960 two-dimensional shell elements. This is a great improvement on the computation efficiency in the analysis of thin-walled structures.

The hierarchy of the identified cross-section deformation modes can also be tested through their participation in the eigenvectors of the thin-walled structure. Fig. 8 shows the amplitude functions varying along the beam axis concerning the first four eigenvectors. These data are derived with the proposed beam model 2. A clear distinction can be observed among the participations of Dominant and Secondary modes. Generally, the participation of a Dominant mode is dozens of times of that of a Secondary mode. Just because of this characteristic, a rational hierarchy becomes possible in organizing

the set of deformation modes using the proposed numbering system. And because of the hierarchy, one is able to select a set of cross-section deformation modes with high priority to form a reduced higher order model. It effectively contributes to the improvement of efficiency in computation, since fewer degrees of freedom needed prevail in the modeling of thin-walled structures.

Moreover, the three-dimensional vibration modes of the thin-walled structure are presented to exhibit the capability of the proposed model in performing three-dimensional analysis. Towards the plotting of the deformed configuration, the displacement field obtained from the proposed model is computed in a “mesh” of sampling points. The mesh is defined over the beam cross-section with 25 points and along the beam axis with 40 points. Thus,  $25 \times 40$  rectangles will be employed to describe the thin-walled structure configuration. To this end, the displacements of these sampling points are obtained from the finite element solution of the proposed beam model and then used to compute the new coordinates of these sampling points. Then in a global coordinate system describing the deformed configuration, these sampling points are interconnected over the cross-section and along the beam axis, respectively. It should be noted that the mesh is just to represent the deformed configuration

and not the discretization adopted for the cross-section analysis.

Fig. 9 provides the comparison regarding the first ten vibration modes of the I-shaped beam. The comparison is divided into ten pairs corresponding to the order of the vibration modes. Within each pair, the left is derived with the proposed beam 2 while the right represents the ANSYS shell result. In general, there is no visible difference between all the ten pairs. This fact proves the capability of the proposed model in predicting the three-dimensional vibration modes of thin-walled structures. Besides, these deformation modes can be observed in the ten actual vibration modes of the thin-walled structure, which strengthens the evidence linking deformation modes and structural behaviors. Simultaneously, the comparison reconfirms the good agreements between the proposed model and the ANSYS shell model.

The results above suggest that the derived deformation modes and the higher order beam model can accurately capture the three-dimensional deformation behaviors of thin-walled structures, and that their hierarchy assignment demonstrates its pivotal role in developing reduced models. Both the accuracy and the efficiency support the necessity of specially determining deformation modes for the dynamic analysis of thin-walled structures. Meanwhile, it is also a successful exploration in giving deformation modes physical interpretation inherited from the structure vibration modes, which may be more valuable for the modeling theory of thin-walled structures.

The proposed procedure together with the higher order model, although involving cross-section discretization and deformation interpolation, is different from either the theory put forward in [26] to obtain final deformation modes through GBT cross-section analysis or the model developed in [33] to derive deformation modes representing higher order effects using the uncoupling procedure. In fact, the authors attempt to avoid both the complex subdivision of deformation modes and the solution of nonlinear eigenvalue problem in determining higher order modes. Instead, a novel procedure has been developed based on three fulcrums: (i) defining a set of basis functions to capture three-dimensional deformation as accurately as possible in an efficient way, (ii) recognizing the variation patterns of amplitude functions within each generalized eigenvector through singular value decomposition, and (iii) decomposing amplitude functions to obtain the set of weights to assemble basis functions in determining cross-section deformation modes. It reduces the requirements on users, and the derived deformation modes naturally own the features of physical interpretation and specific hierarchy, which is further conducive to develop reduced beam models. Besides, it makes it possible to take the structural geometry, material parameters and boundary conditions into account in determining deformation modes, which is in favor of truly reflecting structural behaviors. Most of all, it provides an access to identify deformation modes considering the dynamic behaviors of thin-walled structures.

## V. CONCLUSION

This paper presented a novel procedure to identify cross-section deformation modes of thin-walled structures employing pattern recognition. The main features lie in the capability to be numerically implemented in a general and systematic way and the nature to give the resulting deformation modes physical interpretation together with the hierarchy. In particular, the structural geometry and material parameters as well as boundary conditions are all considered in the determination procedure, to represent actual structural behaviors. It is also featured as a special procedure open to dynamic modeling of thin-walled structures by inheriting the mechanical meaning from actual vibration modes. These properties had also been tested through numerical examples and comparisons with other theories.

Finally, it should be mentioned that available strategies to define basis functions are not confined to the proposed one and that the procedure may be extended to handle arbitrary cross-sections on the basis of some essential improvements. Now the authors plan to develop the procedure to analyze the deformation modes of thin-walled structures with circular cross-sections and curved axes.

## REFERENCES

- [1] Y. Chen, J. Zhang, and Y. Gong, "Utilizing anisotropic fabrics composites for high-strength soft manipulator integrating soft gripper," *IEEE Access*, vol. 7, pp. 127416–127426, Sep. 2019.
- [2] G. Zhu, X. Zhao, P. Shi, and Q. Yu, "Crashworthiness analysis and design of metal/CFRP hybrid structures under lateral loading," *IEEE Access*, vol. 7, pp. 64558–64570, May 2019.
- [3] N.-L. Nguyen, G.-W. Jang, S. Choi, J. Kim, and Y. Y. Kim, "Analysis of thin-walled beam-shell structures for concept modeling based on higher-order beam theory," *Comput. Struct.*, vol. 195, pp. 16–33, Oct. 2018.
- [4] S. T. Dennis and K. W. Jones, "Flexural-torsional vibration of a tapered C-section beam," *J. Sound Vib.*, vol. 393, pp. 401–414, Apr. 2017.
- [5] K. Yoon, P.-S. Lee, and D.-N. Kim, "An efficient warping model for elastoplastic torsional analysis of composite beams," *Compos. Struct.*, vol. 178, pp. 37–49, Oct. 2017.
- [6] S. Capdevielle, S. Grange, F. Dufour, and C. Desprez, "A multifiber beam model coupling torsional warping and damage for reinforced concrete structures," *Eur. J. Environ. Civil Eng.*, vol. 20, no. 8, pp. 914–935, Sep. 2016.
- [7] R. Pavazza and B. Blagojević, "On the cross-section distortion of thin-walled beams with multi-cell cross-sections subjected to bending," *Int. J. Solids Struct.*, vol. 42, nos. 3–4, pp. 901–925, Feb. 2005.
- [8] N.-H. Park, S. Choi, and Y.-J. Kang, "Exact distortional behavior and practical distortional analysis of multicell box girders using an expanded method," *Comput. Struct.*, vol. 83, nos. 19–20, pp. 1607–1626, Jul. 2005.
- [9] Y.-H. Zhang and L.-X. Lin, "Shear lag analysis of thin-walled box girders based on a new generalized displacement," *Eng. Struct.*, vol. 61, pp. 73–83, Mar. 2014.
- [10] F. Cambroner-Barrientos, J. Díaz-del-Valle, and J. A. Martínez-Martínez, "Beam element for thin-walled beams with torsion, distortion, and shear lag," *Eng. Struct.*, vol. 143, pp. 571–588, Jul. 2017.
- [11] F. Naccache and R. El Fatmi, "Numerical free vibration analysis of homogeneous or composite beam using a refined beam theory built on Saint Venant's solution," *Comput. Struct.*, vol. 210, pp. 102–121, Nov. 2018.
- [12] K. Yoon, D.-N. Kim, and P.-S. Lee, "Nonlinear torsional analysis of 3D composite beams using the extended St. Venant solution," *Struct. Eng. Mech.*, vol. 62, no. 1, pp. 33–42, 2017.
- [13] F. Chinesta, P. Ladeveze, and E. Cueto, "A short review on model order reduction based on proper generalized decomposition," *Arch. Comput. Methods Eng.*, vol. 18, no. 4, p. 395, Nov. 2011.
- [14] P. Vidal, L. Gallimard, and O. Polit, "Composite beam finite element based on the proper generalized decomposition," *Comput. Struct.*, vol. 102, pp. 76–86, Jul. 2012.

- [15] A. Sibilleau, A. García-González, F. Auricchio, S. Morganti, and P. Díez, "Explicit parametric solutions of lattice structures with proper generalized decomposition (PGD)," *Comput. Mech.*, vol. 62, no. 4, pp. 871–891, Oct. 2018.
- [16] P. Vidal, L. Gallimard, and O. Polit, "Composite beam finite element based on the proper generalized decomposition," *Comput. Struct.*, vol. 102, pp. 76–86, Jul. 2012.
- [17] W. Yu, D. H. Hodges, and J. C. Ho, "Variational asymptotic beam sectional analysis—An updated version," *Int. J. Eng. Sci.*, vol. 59, pp. 40–64, Oct. 2012.
- [18] F. Jiang, A. Deo, and W. Yu, "A composite beam theory for modeling nonlinear shear behavior," *Eng. Struct.*, vol. 155, pp. 73–90, Jan. 2018.
- [19] D. Harursampath, A. B. Harish, and D. H. Hodges, "Model reduction in thin-walled open-section composite beams using variational asymptotic method. Part I: Theory," *Thin Walled Struct.*, vol. 117, pp. 356–366, Aug. 2017.
- [20] L. Zhang, H. M. Sertse, and W. Yu, "Variational asymptotic homogenization of finitely deformed heterogeneous elastomers," *Compos. Struct.*, vol. 216, pp. 379–391, May 2019.
- [21] E. Carrera and M. Petrolo, "On the effectiveness of higher-order terms in refined beam theories," *J. Appl. Mech.*, vol. 78, no. 2, Nov. 2011, Art. no. 021013.
- [22] Y. Yan, A. Pagani, and E. Carrera, "Exact solutions for free vibration analysis of laminated, box and sandwich beams by refined layer-wise theory," *Compos. Struct.*, vol. 175, pp. 28–45, Sep. 2017.
- [23] A. Pagani, Y. Yan, and E. Carrera, "Exact solutions for static analysis of laminated, box and sandwich beams by refined layer-wise theory," *Compos. B, Eng.*, vol. 131, pp. 62–75, Dec. 2017.
- [24] E. Carrera, A. Pagani, and J. R. Banerjee, "Linearized buckling analysis of isotropic and composite beam-columns by Carrera Unified Formulation and dynamic stiffness method," *Mech. Adv. Mater. Struct.*, vol. 23, no. 9, pp. 1092–1103, Mar. 2016.
- [25] Y. Yan, E. Carrera, A. G. de Miguel, A. Pagani, and Q. W. Ren, "Meshless analysis of metallic and composite beam structures by advanced hierarchical models with layer-wise capabilities," *Compos. Struct.*, vol. 200, pp. 380–395, Sep. 2018.
- [26] R. Gonçalves, M. Ritto-Corrêa, and D. Camotim, "A new approach to the calculation of cross-section deformation modes in the framework of generalized beam theory," *Comput. Mech.*, vol. 46, no. 5, pp. 759–781, Oct. 2010.
- [27] N. Peres, R. Gonçalves, and D. Camotim, "First-order generalised beam theory for curved thin-walled members with circular axis," *Thin Walled Struct.*, vol. 107, pp. 345–361, Oct. 2016.
- [28] R. Bebiano, C. Basaglia, D. Camotim, and R. Gonçalves, "GBT buckling analysis of generally loaded thin-walled members with arbitrary flat-walled cross-sections," *Thin Walled Struct.*, vol. 123, pp. 11–24, Feb. 2018.
- [29] A. W. Ruggerini, A. Madeo, R. Gonçalves, D. Camotim, F. Ubertini, and S. de Miranda, "GBT post-buckling analysis based on the implicit corotational method," *Int. J. Solids Struct.*, vol. 163, pp. 40–60, May 2019.
- [30] R. Bebiano, M. Eisenberger, D. Camotim, and R. Gonçalves, "GBT-based vibration analysis using the exact element method," *Int. J. Struct. Stability Dyn.*, vol. 18, no. 5, 2018, Art. no. 1850068.
- [31] R. Bebiano, R. Calçada, D. Camotim, and N. Silvestre, "Dynamic analysis of high-speed railway bridge decks using generalised beam theory," *Thin Walled Struct.*, vol. 114, pp. 22–31, May 2017.
- [32] R. F. Vieira, F. B. E. Virtuoso, and E. B. R. Pereira, "A higher order beam model for thin-walled structures with in-plane rigid cross-sections," *Eng. Struct.*, vol. 84, pp. 1–18, Feb. 2015.
- [33] R. F. Vieira, F. B. E. Virtuoso, and E. B. R. Pereira, "Definition of warping modes within the context of a higher order thin-walled beam model," *Comput. Struct.*, vol. 147, pp. 68–78, Jan. 2015.
- [34] R. F. Vieira, F. B. E. Virtuoso, and E. B. R. Pereira, "Buckling of thin-walled structures through a higher order beam model," *Comput. Struct.*, vol. 180, pp. 104–116, Feb. 2017.
- [35] R. F. Vieira, F. B. E. Virtuoso, and E. B. R. Pereira, "A higher order model for thin-walled structures with deformable cross-sections," *Int. J. Solids Struct.*, vol. 51, nos. 3–4, pp. 575–598, Feb. 2014.
- [36] R. Bebiano, D. Camotim, and R. Gonçalves, "GBTUL 2.0—A second-generation code for the GBT-based buckling and vibration analysis of thin-walled members," *Thin Walled Struct.*, vol. 124, pp. 235–257, Mar. 2018.



**LEI ZHANG** received the B.S. and Ph.D. degrees in mechanical engineering from the China University of Mining and Technology, Xuzhou, China, in 2011 and 2016, respectively.

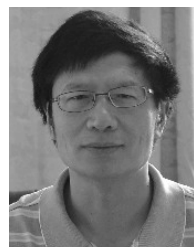
Since 2016, he has been a Lecturer with the College of Mechanical and Electrical Engineering, Hohai University, Jiangsu, China. He is the author of more than 20 articles, and more than 30 inventions. His research interests include applied mechanics, dynamics, vibration control, and modern design theory.



**WEIDONG ZHU** received the dual B.S. degrees in mechanical engineering and computational science from Shanghai Jiao Tong University, Shanghai, China, in 1986, the M.S. degree in mechanical engineering from Arizona State University, Tempe, AZ, USA, in 1988, and the Ph.D. degree in mechanical engineering from the University of California, Berkeley, CA, USA, in 1994.

From 1994 to 1997, he was an Assistant Professor with The Chinese University of Hong Kong, Hong Kong. From 1997 to 1999, he was an Assistant Professor with the University of North Dakota, Grand Forks, ND, USA. Since 2007, he has been a Professor with the Department of Mechanical Engineering, University of Maryland Baltimore County, Baltimore, MD, USA. He is the author of more than 170 archival journal articles. His research spans the fields of dynamics, vibration, control, applied mechanics, structural health monitoring, and wind energy, and involves analytical development, numerical simulation, experimental validation, and industrial application.

Prof. Zhu is a Fellow of the ASME. He was a recipient of the 2004 National Science Foundation CAREER Award, and has five U.S. patents and five ASME Best Paper Awards. He was an Associate Editor of the *ASME Journal of Vibration and Acoustics*, from 2007 to 2014, and has been a Subject Editor of the *Journal of Sound and Vibration*, since January 2018.



**AIMIN JI** received the B.S. degree in mechanical engineering from the Anhui College of Mechanical and Electrical Engineering, Anhui, China, in 1986, the M.S. degree in mechanical engineering from the Harbin Institute of Technology, Harbin, China, in 1991, and the Ph.D. degree in mechanical engineering from the University of Science and Technology of China, Hefei, China, in 2001.

From 1991 to 2005, he was an Associate Professor with the School of Mechanical Engineering, Hefei University of Technology, Hefei. Since 2005, he has been a Professor with the College of Mechanical and Electrical Engineering, Hohai University, Jiangsu, China. He is the author of more than 50 articles, and more than 20 inventions. His research interests include dynamics, optimal design, and biomechanics.

...